Tectonics

RESEARCH ARTICLE
10.1029/2018TC005326

Key Points:
- Three new paleoseismic trenches have been excavated across the Mount Vettore fault system
- Recurrence time for the past five, 2016-like earthquakes (M_w 6.6) is about 1,800 years
- The largest earthquakes sourced by the Mount Vettore fault damaged the most famous monuments in Rome

Supporting Information:
- Supporting Information S1

Correspondence to:
P. Galli,
paolo.galli@protezionecivile.it

Citation:
Galli, P., Galderisi, A., Peronace, E., Giaccio, B., Hajdas, I., Messina, P., et al. (2019). The awakening of the dormant Mount Vettore fault (2016 central Italy earthquake, M_w 6.6): Paleoseismic clues on its millennial silences. *Tectonics*, *38*, 687–705. https://doi.org/10.1029/2018TC005326

Received 11 SEP 2018
Accepted 17 JAN 2019
Accepted article online 25 JAN 2019
Published online 22 FEB 2019

The Awakening of the Dormant Mount Vettore Fault (2016 Central Italy Earthquake, M_w 6.6): Paleoseismic Clues on Its Millennial Silences

P. Galli[1,2], A. Galderisi[2,3], E. Peronace[2,4], B. Giaccio[2], I. Hajdas[5], P. Messina[2], D. Pileggi[6], and F. Polpetta[2,4]

[1]Dipartimento della Protezione Civile Nazionale, Rome, Italy, [2]Istituto di Geologia Ambientale e Geoingegneria, Consiglio Nazionale delle Ricerche, Rome, Italy, [3]Dipartimento di Ingegneria e Geologia, Chieti-Pescara University, Abruzzo, Italy, [4]Dipartimento di Scienze della Terra, Sapienza University of Rome, Rome, Italy, [5]ETHZ-HPK, Zurich, Switzerland, [6]Poseidon Engineering SA, Bellinzona, Switzerland

Abstract The Mount Vettore normal fault ruptured between August and October 2016, sourcing three earthquakes of M_w 6.2, 6.1, and 6.6. The first one caused the death of 299 people, while the entire sequence reached the highest macroseismic intensity levels in Italy since the catastrophic 1915 Fucino event (M_w 7.1). This fault was known to be one of the historically dormant faults of the Italian Apennines, and its sudden activation, not preceded by any foreshocks, has caught people and scientists off guards. We describe here the results from three new paleoseismic trenches opened across splays of the main antithetic fault that ruptured at surface on 30 October together with the 30-km-long Mount Vettore master fault. Data account for six surface faulting events since 9 ka, with a return time of 1.8 ± 0.3 kyr. The penultimate, probably stronger earthquake occurred in Late Roman times, perhaps in 443 AD, when also Rome suffered damage to its monumental buildings. Once again, paleoseismology turns out to be a powerful tool in seismic hazard assessment, especially for earthquakes that recur hundreds or thousands of years apart.

Plain Language Summary Twenty years before the frightful central Italy earthquake of 2016 (M_w 6.6), early paleoseismic trenches revealed the existence and Holocene activity of the Mount Vettore fault system, in the Italian Apennines. New trenches excavated across the 2016 surface ruptures have allowed to define five paleoearthquakes of similar magnitude, the last one occurred in Late Roman period, when also the far monumental building of Rome were damaged. By joining the results of the new paleoseismic analyses with those published 20 years ago, the authors have found that the return time for such a class of magnitude earthquakes is about 1,800 years.

1. Introduction

On 24 August 2016, in the dead of night, 299 persons died under the rubble of the old, stone-masonry houses where they were sleeping at the border among Lazio, Umbria, and Marche Regions (central Italian Apennines). All deaths were caused by the first earthquake (M_w 6.2; RCMT, 2016) of a seismic sequence which is still ongoing after two years. Another M_w 6.1 event occurred on 26 October, whereas the largest one (M_w 6.6) was on 30 October. Earthquakes have been sourced by one of the normal faults dissecting the fold-and-thrust Apennine chain, the Mount Vettore fault system (from now, MVFS). The resulting mesoseismic area was almost entirely located within the hanging wall of the MVFS, reaching the highest macroseismic intensities (Io 11 MCS; Galli, Castenetto, & Peronace, 2017) assigned in Italy since the catastrophic Fucino earthquake (M_w 7.1) in 1915 (Io 11 MCS; Molin et al., 1999).

Although this area was classified as Seismic Zone 1 (the highest level in the Italian code), we could say that the earthquake took place unexpectedly, at least from a couple of points of view: one pertaining to the human perception of hazard and the other related to our scientific knowledge. This is because the first shock was not preceded by any seismic swarm, or even by single foreshock in the months before, as sometime observed in the seismic history of Italian strong sequences. In turn, it was sourced by a well-known active fault, which was classified as silent or dormant fault (Galli & Galadini, 1999), that is, a fault with geological evidence of Holocene surface ruptures, yet not associated with historical earthquakes. Since silent faults in

Figure 1. The impressive 30 October 2016 surface faulting along the antithetic San Lorenzo Fault. Here the fault crossed and destroyed a dirt road, with an offset of ~1 m. Note the rock-fault scarp that crops out just above the coseismic free-face (right side; car and persons for scale). Photo taken 3 hr after the earthquake.

the Apennines have long recurrence times (>1.5 kyr), longer than all the other seismogenic sources that have ruptured twice or more during the historical record, most earthquake geologists would not have thought to see one of these faults rupturing during their life.

In this paper we try to unravel the Holocene seismic history of the MVFS, enhancing and integrating the results gathered in previous paleoseismic analyses (Galadini & Galli, 2003). In doing this, we dug three new trenches across as many fault splays that ruptured at surface on 30 October 2016 that, all together, form the main antithetic fault of the MVFS (San Lorenzo fault; from now, SLF; Figures 1, 2b, and 2d). We have investigated this segment because it affects and dams small Quaternary alluvial basins that were prone to host fine, datable deposits. In contrast, the MVFS master fault runs mainly along the highest slopes and crests of the Sibillini mountain ridge (Calamita et al., 1992), offsetting mostly coarse carbonate slope deposits in the hanging wall versus Mesozoic limestones in the footwall, that is, materials that are not suitable for paleoseismology.

At the moment, one possible weak point of our choice is that whereas the master fault should partly rupture at surface even for M_w 6.2 earthquakes (see the centimetric offset of the 24 August 2016 event; Galli et al., 2016; Civico et al., 2018), it is possible—although not sure—that the antithetic and synthetic faults do not (i.e., the Prate Pala splay recorded only a faint crack on 24 August 2016). In fact, it is known that antithetic and minor synthetic normal faults often represent accommodation structures within the master fault hanging wall block (Figure 2d; see Yeats et al., 1997 with references). Thus, waiting for future excavations in some key sites that we have identified in small basins formed at high elevations, where the master fault doubled the crest of the Sibillini ridge (to be performed through an airborne excavator), here we assume that for $M_w > 6.5$ events (i.e., those predominantly investigated by paleoseismology), the antithetic San Lorenzo Fault slips together with the master fault, even with smaller offset.

2. Background

2.1. Active Tectonics and Seismicity of Central Italy

The Neogene-Quaternary kinematic evolution of the Italian Alps-Apennines orogen was driven by the interaction between the Eurasian and African plates, which are currently converging at a rate of 6 mm/year along a NW-SE direction (e.g., Battaglia et al., 2004). The existence of Adria, a fragmented promontory of Africa into Eurasia (D'Agostino et al., 2008), led to a complex plate collision dynamic, as indentation of Adria toward the NE progressively transferred the Africa motion to the regions surrounding the Adriatic onland. This resulted in active shortening all along the Adria borders, accompanied by strong, compressive, and transpressive seismic activity. In contrast, the seismicity along the Apennine chain (Figure 2a) is attributable to a complex and debated geodynamic process which is linked, on the one hand, to the flexure-hinge retreat of the currently west subducting Ionian-Adriatic slab and, on the

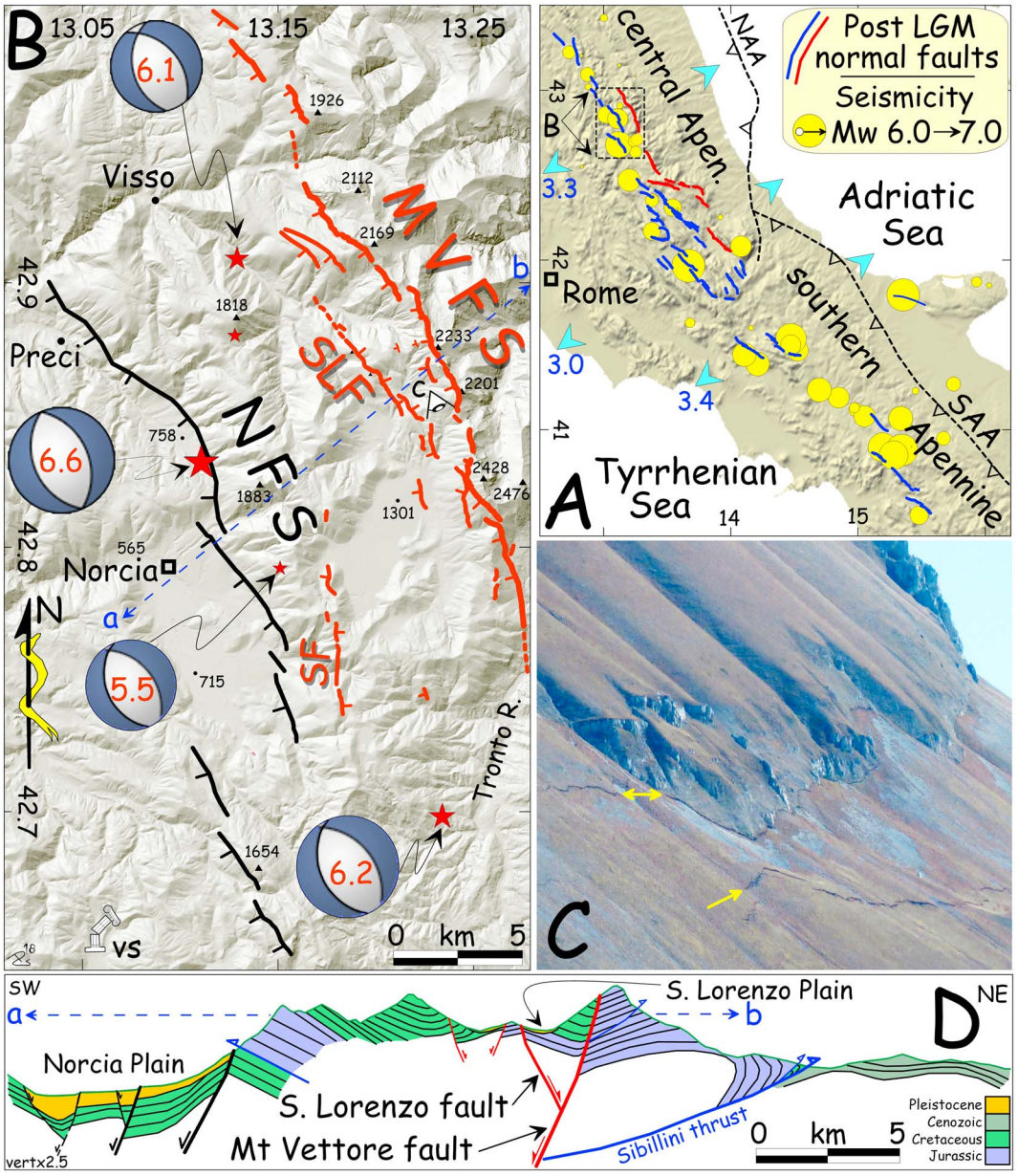

Figure 2. (a) Shaded relief map of central-southern Apennines showing >M_w 6.0 historical earthquakes and post Last Glacial Maximum faults (red, historically dormant faults). NAA and SAA, northern and southern buried front of fold-and-thrust chain. Cyan arrows—pair, GPS extension (mm/year; from Galli & Peronace, 2014). (b) Shaded relief map of the area crossed by the Mount Vettore fault system (MVFS, in red; SLF and SF, San Lorenzo and Mount Serra antithetic faults) and by the Norcia fault system (NFS, in black). Blue beach balls are the focal mechanisms of the 2016 central Italy sequence (GFZ solutions); vs ruins of Villa San Silvestro temple (a-b section in (d)). (c) View looking south of the impressive, ~25-m-high, rock-fault scarp affecting the western slope of Mount Vettore ridge (see point of view c in (b)). Double yellow arrow points to the 2016 rejuvenation of the fault at the bottom of the fault scarp (up to 2-m-high; Figure S3); yellow arrow indicates a secondary splay in the hanging wall. (d) Schematic geological section (a-b in (b)) showing the geometrical relation between the main Mount Vettore fault and the antithetic San Lorenzo splay.

other, to the post-orogenic gravitational collapse of the chain (Carminati et al., 2012; Doglioni et al., 1994; D'Agostino et al., 2001; Patacca et al., 1990, 2008).

Following the fold-and-thrust structuring of the inner chain, since Late Pliocene NE-SW extension progressively affected central Apennines, where SW dipping normal faults drove the opening of Quaternary, intermontane basins (Boncio et al., 2004; Bosi et al., 2003; Galadini & Galli, 2000; Galli et al., 2010; Giaccio et al.,

2012; Roberts & Michetti, 2004). Extension is currently focused along the axis of the chain, where NW-SE normal faults generate the strongest earthquakes. According to GPS data (Figure 2a; D'Agostino, 2014), extension rate in central Apennines ranges between 2.5 and 3.3 mm/year, with a strip of steeper gradient enveloping all the primary, western active normal faults (Galli & Peronace, 2014).

Apennine active faults may be grouped into two main systems (Galadini & Galli, 2000): one roughly running along the chain axis (Western Fault System, WFS from now; Figure 2a) and the other closer to its eastern front (Eastern Fault System (EFS)). All these faults are arranged in systems of en echelon segments, which are 2–20 km long (Boncio et al., 2004; Calamita & Pizzi, 1994; Cello et al., 1997; Galli et al., 2011, 2016; Galadini & Galli, 2000; Lavecchia et al., 1994; Pizzi et al., 2002; Roberts & Michetti, 2004). The maximum fault system length rarely exceeds 30 km, whereas—according to traditional trench paleoseismology—faults are characterized by 0.5–2.5-kyr recurrence time for $M_w > 6.3$ earthquakes (Galli et al., 2008, 2011, 2015, 2016, 2018). However, studies from ^{36}Cl exposure dating (Benedetti et al., 2013) have hypothesized that large earthquakes in central Italy do not repeat periodically, but rather in supercycles encompassing several events that are strongly controlled by fault interaction. Similar studies let Cowie et al. (2017) hypothesize a temporal variability in fault slip rates (and thus earthquake occurrence) across the two flanks of central Italian Apennines, with the recent seismic activity representing just a snapshot of a more complex deformational framework of the chain.

Undoubtedly, the distribution of epicenters of $M_w > 6.0$ earthquakes in the past 1,000 years (Figure 2a) suggests that their causative structures lay among the WFS, as demonstrated also by paleoseismological studies (e.g., in Galli et al., 2008; Galli & Peronace, 2014) that link most of the $M_w > 6.5$ historical event to individual fault. In turn, the EFS, although responsible for surface faulting during Late Pleistocene–Holocene, has been defined as historically silent (Galadini & Galli, 2000). Among these faults, the MVFS has been dormant for a long period (Galli & Galadini, 1999), until it dramatically woke up between 24 August and 30 October 2016.

In the investigated area, written sources account for several $M_w > 5.5$ earthquakes that struck the villages located westward of the WFS, and in particular those in the hanging wall of the primary Norcia fault system (NFS in Figure 2b), paralleling the MVFS. Almost all these events were sourced by the three main NFS segments that, rupturing independently (year 1599, M_w 6.1; 1719, M_w 5.6; 1730, M_w 6.0; 1859, M_w 5.7; 1979, M_w 5.8), grouped (1328, M_w 6.5) or all together (1703, M_w 6.9) caused the repeated destructions of dozens of villages in the last millennium (see details and maps in Galli et al. (2018)).

Conversely, no historical earthquakes have been associated with the MVFS so far, with the exception of few $M_w < 4$ events on record during the instrumental period, all with focal mechanisms evidencing NE-SW extension accommodated by NW-SE trending planes (TDMT, 2018). For instance, a M_w 3.6 event in 1985 matching the epicenter of the 24 August 2016, sparse M_w 3.6–3.9 events in the Castelluccio di Norcia Plain (between 2007 and 2012), and a M_w 3.8 event in November 1999, matching the 2016 mainshock, even with a comparable N155° focal plane.

2.2. Clues on the Activity of the MVFS and Its 2016 Surface Rupture

The MVFS is a ~30-km-long, N165° striking normal fault, made up of dozens of 1–3-km-long, en echelon segments, with several synthetic and antithetic splays in the hanging wall, the main one being the 5-km-long, antithetic SLF (Figures 2b, 3, and, 4). On the basis of the prominent rock fault scarp facing the Piano Grande (Mount Redentore slope; Figures 2c and 3), Calamita et al. (1992) first hypothesized a recent activity of the master fault, whereas conclusive geological evidence for the Late Pleistocene–Holocene activity were definitively provided since Galli and Galadini (1999).

These authors identified the existence of a subdued, 1.5-km-long fault scarp paralleling the main Mount Redentore fault segment that affects a polygenic alluvial fan in the NE corner of the Piano Grande (Prate Pala splay in Figure 3). The fan is composed of five overlapping alluvial phases that were dated between the onset of the Last Glacial Maximum (LGM; 26.5–19.0 ka; Clark et al., 2009) and the Upper Holocene, with the fault scarp crossing obliquely the latest two fan lobes (IV-V, Figure 3; Galadini & Galli, 2003). The most recent one is attributable to a widespread cold phase known in central Apennines for being subsequent to 4445–4150 BP (Giraudi, 2005), matching the so-called 4.2 global drought/cooling event, which lasted between 4.3 and 3.8 ka (Zanchetta et al., 2012). In turn, fan IV could be attributed to the regional Mount Aquila stadial (10–11 kyr BP; Giraudi, 2003).

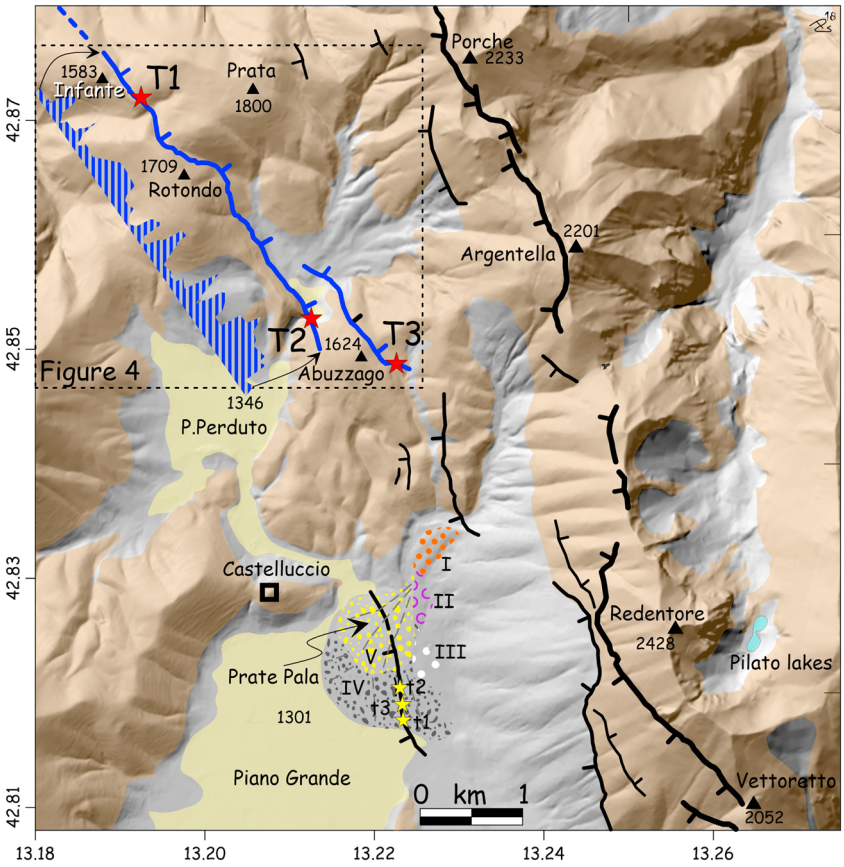

Figure 3. Shaded relief map of the studied area. Bold black lines are the middle part of the main Mount Vettore fault segments that ruptured at surface on 30 October 2016; thinner black lines are the synthetic and antithetic splays which also ruptured during the earthquake. Blue line is the main antithetic fault (San Lorenzo fault: blue dashed graph shows the variation in the magnitude of the along-fault coseismic rupture; 0–1.2 m offset range). Light brown, Meso-Cenozoic, marine carbonate succession; yellow, Holocene, fine-alluvial deposits (lacustrine); gray, Late Pleistocene slope deposits, talus, and alluvial cones. I–V, polyphasic alluvial fan of Prate Pala (Last Glacial Maximum–late Holocene). Red stars, trenches in this paper (T1–3). Yellow stars, trenches (t1–3) in Galadini and Galli (2003).

Topographic leveling made by Galadini and Galli (2003) revealed that the scarp height was ~3 m in fan IV and ~2 m in fan V, yielding a local slip rate of 0.3 ± 0.02 and 0.5 ± 0.05 mm/year, respectively (Figures S1 and S2). These authors dug also three paleoseismological trenches across the scarp affecting fan V (Figure 3), finding evidence for two surface rupture events in the Upper Holocene, plus others occurred after the onset of LGM. More specifically, the ultimate event was dated a long time after 4 kyr BP, shortly before 240–480 AD (tentatively after 50–265 AD; Galli, Castenetto, & Peronace, 2017). The recurrence time was not evaluable, although surely shorter than 4.7 kyr.

Today, plentiful seismological, geodetical, geological, and macroseismic papers (Cheloni et al., 2017; Chiaraluce et al., 2017; Ferrario & Livio, 2018; Galli, Castenetto, & Peronace, 2017; Pizzi et al., 2017; Scognamiglio et al., 2018; Villani et al., 2018) have demonstrated that the MVFS is undoubtedly the seismogenic structure responsible for the seismic sequence started on 24 August 2016. The entire MVFS ruptured at surface for a length of ~30 km on 30 October, reactivating the surface breaks formed along the southern and northern tips on 24 August and 26 October, respectively (Civico et al., 2018). The coseismic ground displacement was abrupt, with the main vertical offset formed in a couple of seconds immediately after the beginning of the hypocenter rupture (6–8 s; Wilkinson et al., 2017), demonstrating that surface rupture was the result of dynamic earthquake slip and not of shaking-induced gravitational processes. The coseismic vertical offset reached a maximum of 2.2 m on the Mount Redentore slope, where the free-face was constantly above 1 m along a couple of kilometers, and added to the 20–30-cm displacement formed the 24 August event (Figure S3). Generally, we measured a vertical offset ranging between 0.25 and 0.75 m along the main

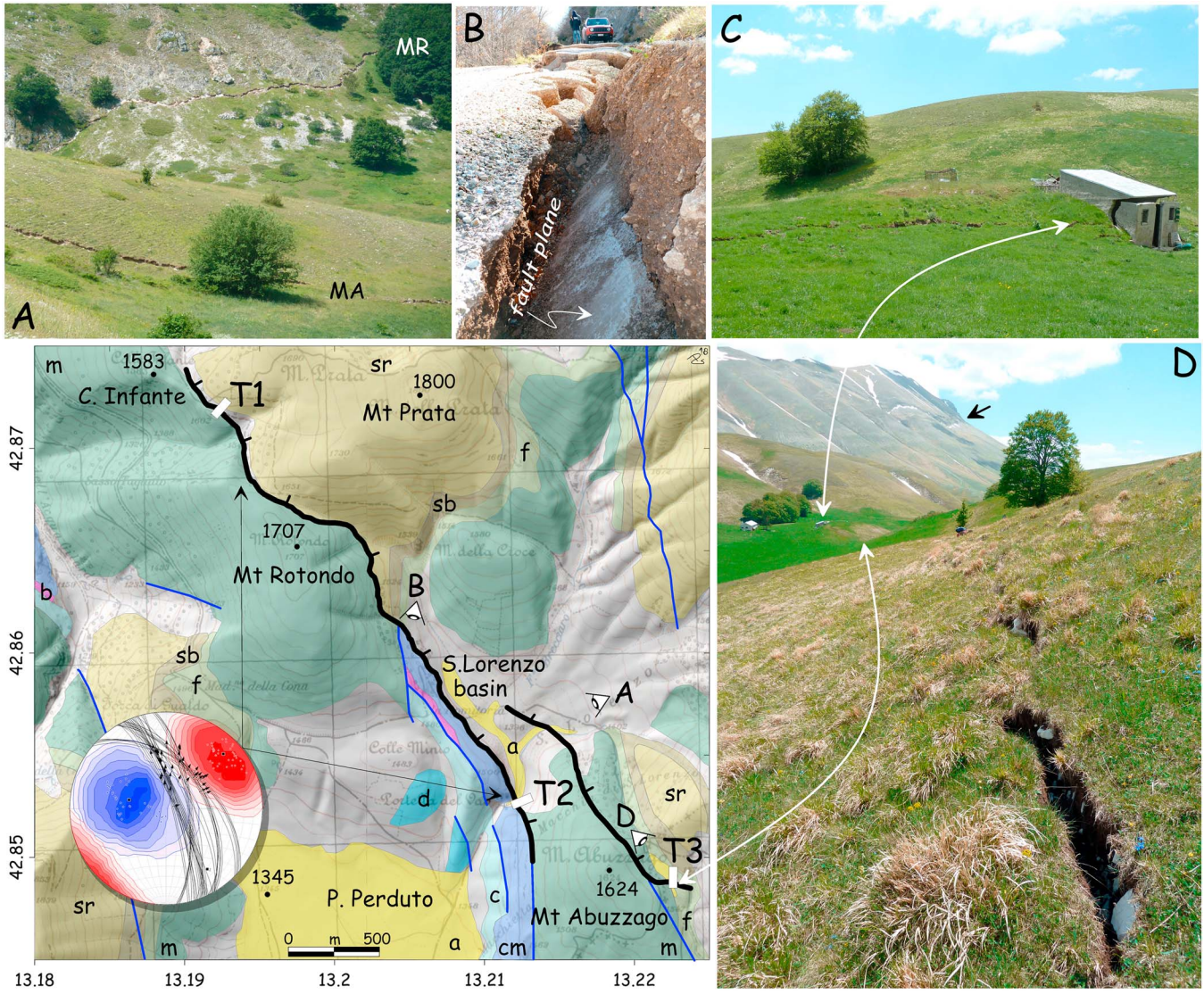

Figure 4. Geological map (modified after Pierantoni et al., 2013; base 1:25,000 IGM map and 10-m shaded relief DTM) of the area affected by the antithetic, San Lorenzo Fault (bold black line: 30 October surface faulting). T1–3, sites of paleoseismological trenches in this paper. A, B, and D: point of views of panels (a), (b), and (d). Meso-Cenozic formations: Cm, Calcare Massiccio; b, Bugarone; c, Corniola; d, Calcari diasprigni; m, Maiolica; sb, Scaglia Bianca; f, Marne a fucoidi; sr, Scaglia rossa. (a) Late Quaternary, fine alluvial-lacustrine deposits; gray: slope deposits, alluvial fan, landslide bodies, talus. The stereogram evidences fault planes, striae trend (arrows), and *P* axis (blue) and *T* axis (red) density. (a) View looking west of the fault step-over between the Mount Abuzzago (MA) and Mount Rotondo (MR) segments. (b) View looking south of the surface rupture across a dirt road over San Lorenzo basin (morning of 30 October 2016; same as Figure 1 site). Note the rock fault plane below the road step. (c) View looking south of the fault affecting a small house near trenching site T3. (d) View looking southeast of the surface faulting along the Mount Abuzzago segment. The black arrow indicates the Mount Vettore master fault along the Mount Redentore slope (see Figure 2c).

segments, from the slopes facing the Tronto River to the south to the northernmost endpoint (Figure 2b), with an arithmetic average displacement of 0.37 m calculated by Brozzetti et al. (2019). Coseismic offset was observed also along the Prate Pala scarp, where the net vertical offset did not exceed 19 cm, ranging between 3 and 10 cm all along 1 km of rupture length (e.g., in Villani & Sapia, 2017).

Importantly, surface ruptures occurred extensively along the antithetic, 5-km-long SLF, which comprises two main segments (Colle Infante-Mount Rotondo and Mount Abuzzago; Figure 4) with a left en echelon step in map view (~0.4 km) and a 0.6-km overlap (Figures 3 and 4). According to the geological section shown in Figure 2d, we estimate that the SLF joins the main Mount Vettore fault at ~1.2 km of depth.

Other discontinuous surface ruptures with offset up to 20 cm were surveyed along the southernmost, 4-km-long antithetic fault of Mount Serra (SF in Figure 2b). This fault is well highlighted at depth by

hypocenter alignment (Chiaraluce et al., 2017), and was responsible for the faulting of the 4,400-m-long San Benedetto tunnel (National Road 685), where we measured 20-cm-vertical and 13-cm-left offset (see details in Figure S4).

3. Results

The segments composing the MVFS master fault run at high elevation (1,600–2,200 m above sea level (asl)), mainly along the steep west slopes of the Sibillini Range, along the sharp rocky crest, or eastward of the ridge (Figure 3). This is why, so far, paleoseismological analyses focused on the only accessible splay of Prate Pala, which is also the only one surely affecting post-LGM alluvial-colluvial deposits. The manner in which the synthetic and antithetic splays were revealed at surface on 30 October has allowed the identification of a number of new sites where Late Pleistocene sediments are preserved, and therefore suitable for paleoseismological trenching. We present here the results gathered from three trenches opened between May and June 2017 along the SLF (Figures S5–15): two across the Mount Rotondo-Colle Infante segment (T1, Colle Infante site; T2, Portella di Vao site; Figure 4) and one across the Mount Abuzzago segment (T3, Capanna Ghezzi site; Figure 4d).

Along the SLF southern segment, coseismic offsets were small (1–35 cm) and discontinuous, whereas they were continuous and larger (up to 1.2 m) along the longer (~3.5 km), northern segment, with average throws between 0.3 and 0.8 m (see offset graph in Figure 3). The SLF plane has an average N335° strike, 70° dip, striae trend N13°, and plunge 59°, suggesting a *T* axis N47° with a plunge of 21° (Figure 4).

In the Prate Pala area we performed topographic leveling along the paths of two profiles that Galadini and Galli (2003) made in 2001, as well as along one made in 2005. Using the GPS coordinates of the old profiles, and the same instruments of the time, we compared the 2001 ground profile with that following the 2016 earthquake (Figure S1). Given the error added by agricultural reworking of the ground surface, the post-2016-faulting scarp has grown by 0.5 ± 0.1 m with respect of the 2001 profiles (alluvial fans IV-V; Figure 3), and by 0.7 ± 0.1 m with the respect to the 2005 profile (alluvial fan IV, where we measured 0.19 m of 2016 coseismic offset). We will discuss these results later, together with the outcomes of the trench analyses.

3.1. The Colle Infante Trench (T1)

The trench site lays between Colle Infante and Monte Prata, at an elevation of ~1,590 m asl (Figures 4 and 5). Here the SLF downthrows the westward dipping slope of Monte Prata, generating a morphological 20–30-m-wide flat saddle in its hanging wall, with the Colle Infante-Mount Rotondo ridge in the footwall. The fault juxtaposes the Maiolica formation calcilutites (Tithonian-Albian) against the Scaglia Rossa formation Marly limestones (Turonian-Lutetian), with the saddle filled by the scree deposits made at expense of both formations.

In order to check the thickness of these loose deposits in the SLF hanging wall, we performed a 72-m-long Electrical Resistivity Tomography profile, with 1-m-spaced electrodes (Figures 5a and 5b) that showed evidence of high-resistivity bodies (limestone) both in the entire SLF footwall, and at depth in the hanging wall. The latter is mantled by 2–4-m-thick low-resistivity materials that we interpreted as recent loose slope deposits and colluvia. Topographic leveling across the fault scarp revealed the presence of a net inflection point (in the sense of Wallace, 1980) located ~8 m uphill, associated with a 1.4-m vertical separation (Figure 5c). This suggests the occurrence of a previous ~0.8-m-high surface faulting event, the inflection point representing its retreated coseismic free-face (e.g., in Galli et al., 2014).

The 12-m-long and 3-m-deep trench was opened with a Holland-EX-55 excavator starting from the step formed on 30 October that here was constantly 0.5–0.8-m-high (Figure 5b). The excavation (Figure 6) exposed clinostratified, slope-derived gravels in a silty matrix (unit 7) faulted against coarse gravels (7a, 6) and limestone (8). In the fault zone, coarse gravelly colluvial wedge (6) are faulted and buried below slope deposits (7b) and a younger colluvial wedge (5). Upward, the hanging wall sequence contains an important erosional surface (es2), whereas all faults are sealed by a dark brown paleosol (3), filling postholes dug inside unit 7. The rocky footwall (9) is separated by the downthrown block by an along-fault open fissure which was rapidly infilled by loose gravel (1), similarly to an older filled fissure (4).

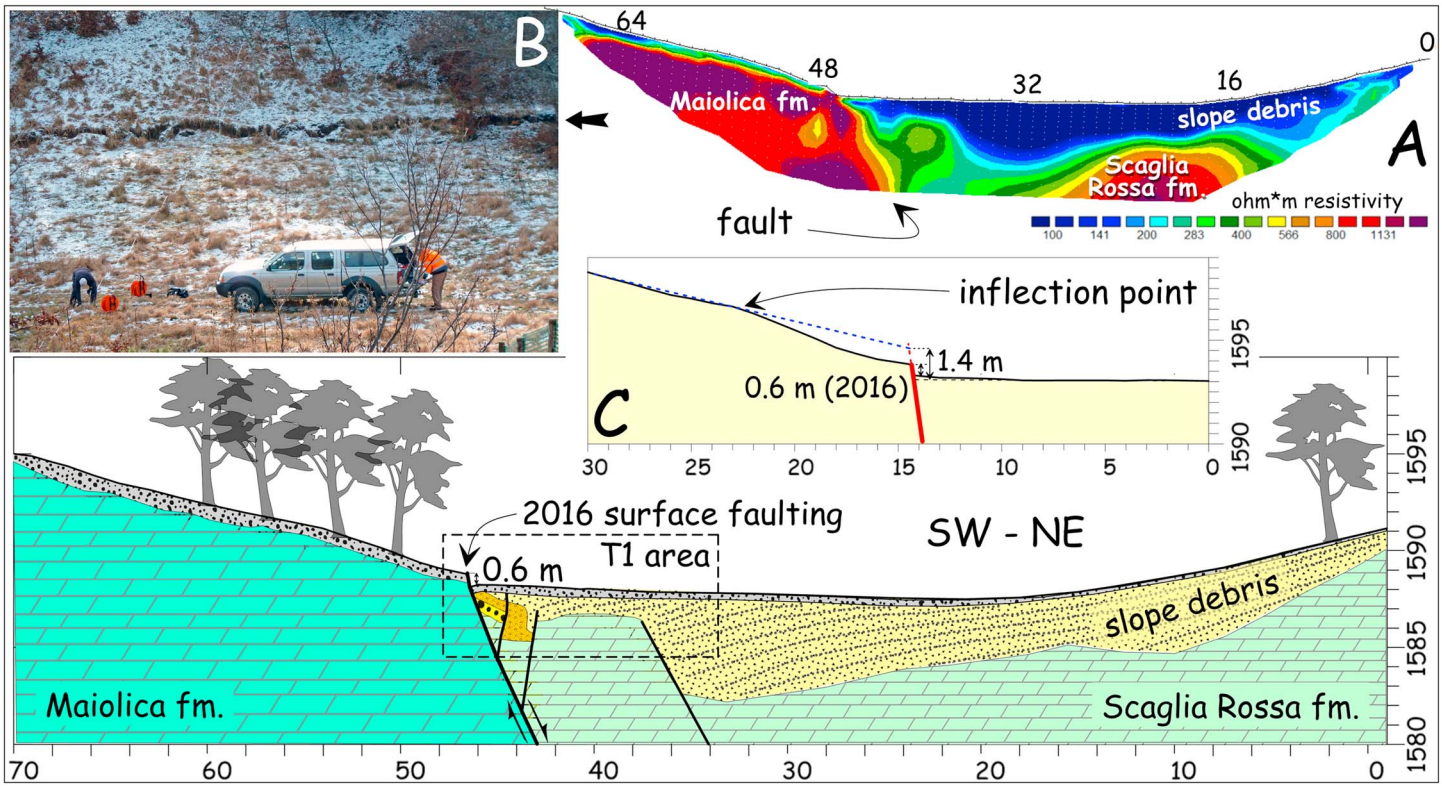

Figure 5. (a) Geological section across the San Lorenzo Fault at T1 site (Figures 3 and 4). The geometry of the buried units has been imaged using the Electrical Resistivity Tomography of inset a (Werner-Schlumberger method) coupled with data observed in trench (see Figure 6 for details). (b) View looking SW during the Electrical Resistivity Tomography acquisition, with the 30 October 2016 surface rupture (0.6–0.8 m) in background (black arrow). (c) Ground leveling evidencing a cumulative 1.4-m vertical separation of the fault scarp, accounting for both the 2016 and a previous event.

The age of the succession has been defined by five AMS dates (Table 1). Paleosol 3 (Figure 6) was probably buried during an early Middle Age cold period (pedogenized gravels, unit 2), after 690–875 AD, whereas the underlying colluvia and slope gravels deposited during the Holocene, between 11 and 5 ka at least.

By comparing the stratigraphical relationships among the units, we defined five, nonconsecutive faulting events and their associated offsets (note that events numbers herein reported refer to the succession of paleoearthquakes deriving from the three trenches, as discussed later). The last one is the 2016 event (E1), with a vertical offset of 60 cm and the formation of an open fissure facing the main fault, which was rapidly infilled by carbonate gravels (1). Another event (E2) is revealed by the faulting of units 5 and 6 along a synthetic splay, with the formation of an open fissure filled by unit 4, and buried by unit 3. A previous event (E4) might be suggested by the presence of a wedge-shaped deposit (unit 5, colluvial wedge), interbedded within the sedimentation of unit 7b. Another event (E5) is testified by the faulting of unit 7-7a due to an antithetic splay, and by the formation of a huge colluvial wedge (6) burying the units below. The same fault splay shows a larger offset of the bottom of unit 7, suggesting, tentatively, the presence of a further event before (E6).

3.2. The Portella di Vao Trench (T2)

We opened trench T2 at the southern endpoint of the Colle Infante-Mount Rotondo segment, where the fault crosses the outlet of the 1-km-long intermontane San Lorenzo basin (Figure 7a), damming its drainage toward the Piano Perduto basin (Figures 3 and 4). Due to the presence of fine, organic sediments, here we collected the most robust results as far as previous surface ruptures are concerned.

The 2016 SLF rupture reached the highest slip values along the preexisting slickenside facing this basin, with vertical offsets up to 1.2 m (Figure 3) and the continuous exhumation of a polished fault plane carved within the Calcare Massiccio formation (Figures 7c and 7d). The vertical offset abruptly decreased to 0.25 m in the alluvial plain, where the rupture branched into two to three overlapping splays. Here the ground surface is

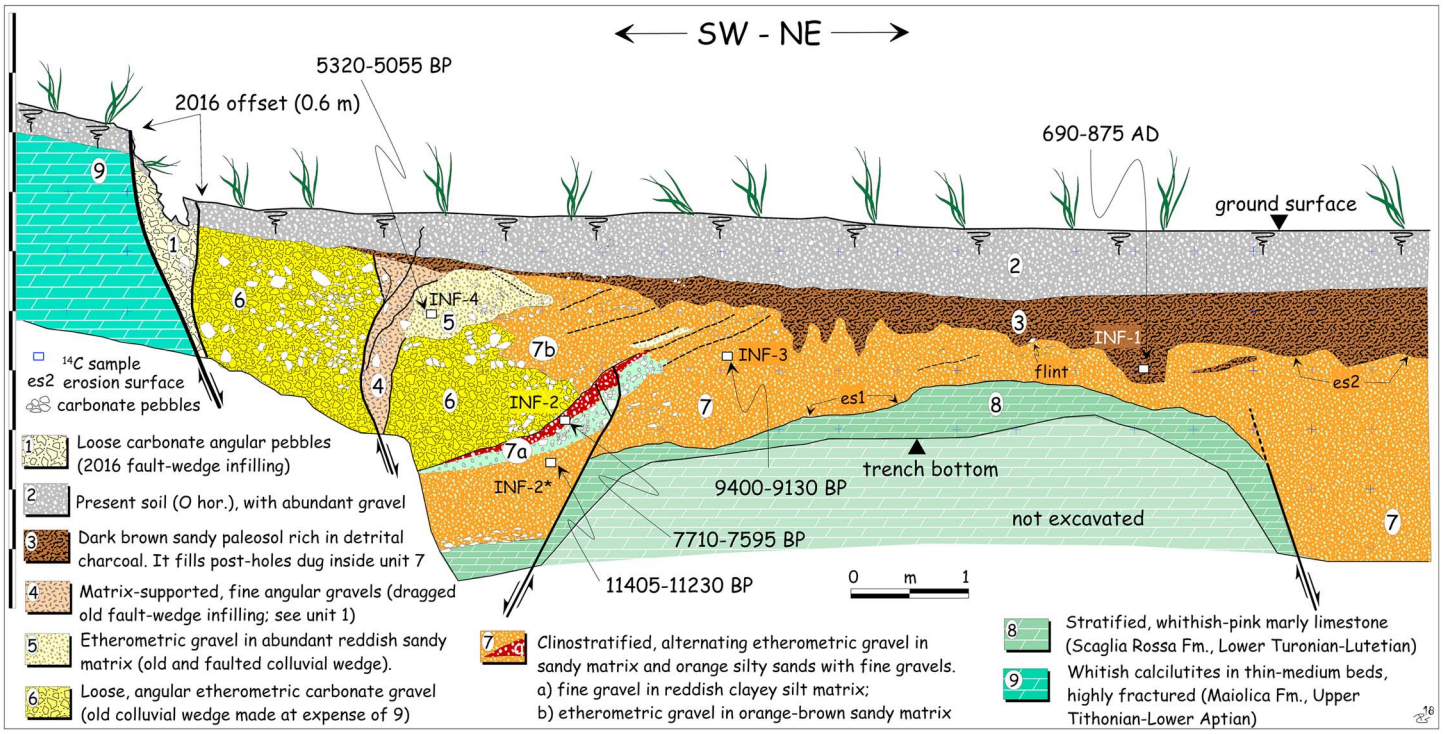

Figure 6. Geological sketch of the northern wall of T1 (Colle Infante area). In addition to evidence of the 2016 event, four previous, nonconsecutive events have been defined in this trench, as suggested by the presence of colluvial wedges and differential offsets of units.

gently warped by these splays, which partly show a vertical offset and partly continue as open fissures with lateral displacement (Figure 7b). We carried out a 30-m-long ground leveling transect across the basin threshold that showed a vertical separation of 1.3 m of the top surface of the basin, which probably represents the 2016 deformation superimposed on previous events (Figure 7).

Table 1
Laboratory Ages of Samples Considered in This Study

Trench	Sample	Wall	Laboratory	Dated Material	$d^{13}C$	Measured Age (BP)	2 s cal. 95%
T1	INF-1	N	ETH-80699	Charred material	−31.1	1236 ± 22	690–875 AD
	INF-2	N	BETA-471455	Organic sediment	−23.4	6830 ± 30	7710–7595 BP
	INF-2*	N	ETH-80700	Organic sediment	−24.1	9914 ± 36	11,405–11,230 BP
	INF-3	N	ETH-80701	Organic sediment	−21.1	8265 ± 27	9400–9130 BP
	INF-4	N	ETH-80702	Organic sediment	−30.1	4564 ± 30	5320–5055 BP
T2	SLOR-1	S	ETH-80703	Organic sediment	−28.2	1662 ± 22	340–420 AD
	SLOR-1 s	S	BETA-483825	Organic sediment	−25.4	1550 ± 30	420–575 AD
	SLOR-2	S	SacA-51329	Organic sediment	−26.6	2455 ± 30	2705–2365 BP
	SLOR-4	S	ETH-80704	Organic sediment	−30.8	3357 ± 23	3645–3560 BP
	SLOR-5	S	SacA-51330	Organic sediment	−23.7	2000 ± 30	55 BC–70 AD
	SLOR-6	N	ETH-80705	Charred material	−28.8	4880 ± 25	5650–5590 BP
	SLOR-7	N	ETH-80706	Charred material	−27.2	3988 ± 24	4520–4415 BP
	SLOR-7b	N	BETA-471456	Organic sediment	−25.4	3860 ± 30	4410–4160 BP
	SLOR-9 s	N	SacA-51331	Organic sediment	−23.7	3860 ± 30	4410–4160 BP
T3	GHEZ-1	E	ETH-80696	Charred material	−24.3	2213 ± 23	2310–2155 BP
	GHEZ-2	E	ETH-80697	Organic sediment	−23.2	7712 ± 26	8545–8425 BP
	GHEZ-4	E	ETH-80698	Organic sediment	−14.9	16493 ± 46	-
	GHEZ-6	E	BETA-471454	Charred material	−24	2040 ± 30	120 BC–25 AD
	GHEZ-6 s	E	SacA-51326	Charred material	−24.6	2030 ± 30	115 BC–50 AD

Note. The 2σ calibration made with software Calib (execute version 7.1, retrieved from http://calib.qub.ac.uk/calib/). (ETH: ETH/AMS Facility, Zurich, Switzerland; BETA: Beta Analityc, Miami, USA; SacA: CEA Saclay, Gif sur Yvette, France).

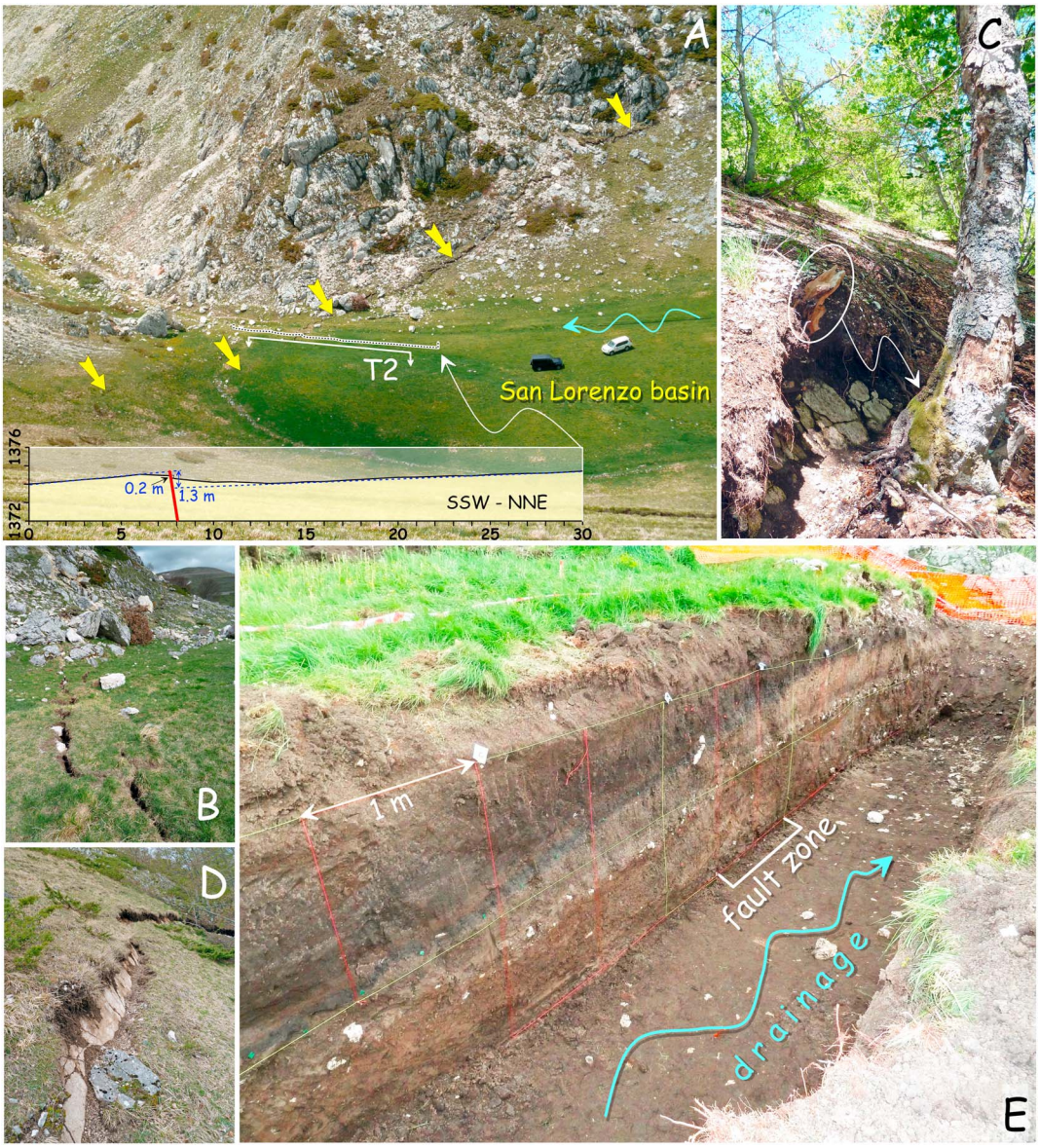

Figure 7. (a) View looking west of the southernmost sector of the San Lorenzo basin; yellow arrows point to the 2016 surface faulting. Here the repeated, coseismic downthrow of the hanging wall has induced the ephemeral swamping of the basin, and caused the formation of palustrine-lacustrine deposits. Dotted line indicates the ground profile path (0.2-m coseismic offset; 1.3 m, cumulated warping). White line is the trench T2 (Figures 7e and 8). (b) Surface ruptures across the basin outlet (site of trench T2). (c) Surface faulting cutting through a beech tree (ellipse highlights the tree-trunk side resting in the footwall). (d) The 80-cm-high free-face formed along the basin border. (e) View looking south of the southern wall of trench T2 (1-m-spaced grid). Note the gentle warping of the lacustrine strata dipping toward the opposite side of the basin outlet (right), which was caused by the downthrown of the hanging wall (left).

The trench—dug with a Hitachi-EX-215 excavator—was 18-m-long and 4.5-m-deep, and was opened across two en echelon fault splays with 1-m-wide step-over. The northern one had a vertical offset of 0.25 m and a horizontal component of 0.2 m; the southern one was characterized by an open fissure of 0.1 m, 0.1–0.2 m of horizontal slip, absence of net vertical offset, although a gentle warping of the ground surface was clearly visible (Figures 7a, 7b, and 7e). Since the two trench walls were 3 m apart, we investigated both the brittle deformation on the northern wall, and the ductile deformation on the southern one, comparing the effects of the two within the same trench.

Deposits exposed within the trench were fine sands, silts, and clays, with interbedded thin levels of coarse-to-medium gravels, the latter mostly observed on the northern wall (toward the stream axis), where we also reached the rocky basement of the footwall, at a depth of ~3 m. Sediments are mainly of palustrine-

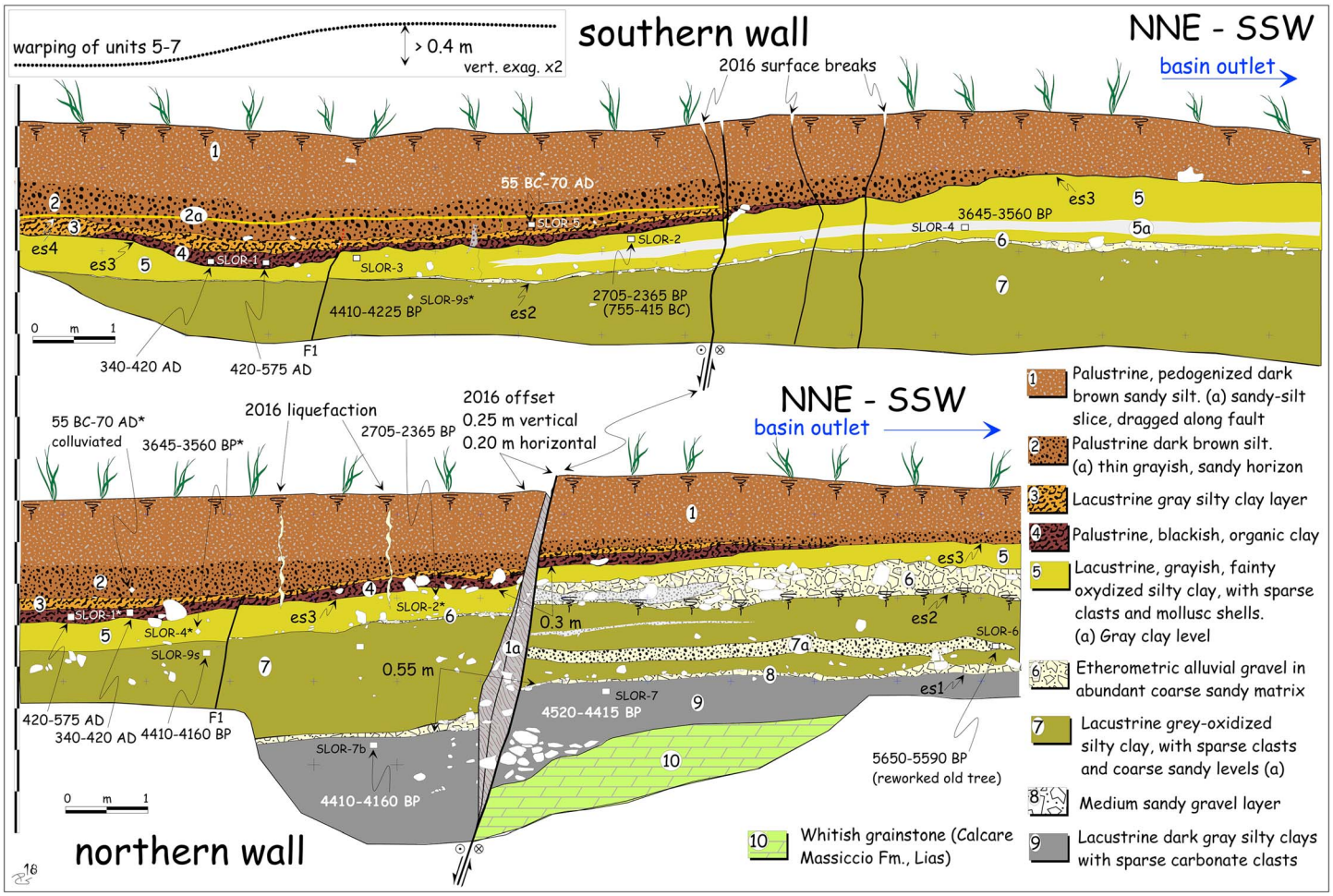

Figure 8. Geological sketch of northern (mirrored image) and southern walls of trench T2. Note the prevailing ductile deformation in the southern wall (top) with respect to the northern, where brittle deformation mainly occurs. In both cases, the resulting topography is at odd with the natural drainage of the basin.
A couple of AMS ages look out of sequence, as in unit 7a where a big charcoal fragments (SLOR-6; 2–3 cm) of an old tree (5.5 ka) has been transported by an alluvial event (unit 7a) inside a younger unit (7). The same is for sample SLOR-5, which is an old colluviated charcoal, fallen in the younger unit 2.

lacustrine origin, partly laminated, and with a primary, subhorizontal layering. They are truncated upward by four erosional surfaces that are also highlighted by alluvial sandy gravels. A thick pedogenized colluvial layer caps the entire sequence. Considering that higher-energy deposits (coarse sand and gravel lenses) are not isopachous, due to the lateral component of the fault they appear with different thickness across the two sides of the fault.

The chronology of the sequence has been established by nine AMS ages within the Upper Holocene (Table 1). The top of the lowermost darkish clayey, lacustrine deposit (unit 9 in the northern wall; Figure 8) has been dated between ~4.5 and 4.3 ka, an age close to that of the overlying silty, marshy unit 7 (~4.3 ka), which is separated from 9 by a sandy gravel horizon (8). The top of unit 7 is eroded and capped by a thin sandy gravel layer (layer 6; much thicker in the footwall side of the northern wall) that is overlaid by laminated, gray lacustrine clayey silts (unit 5) dated between ~3.6 and 2.5 ka. Upward, unit 5 is truncated by a deep, concave erosional surface, successively infilled by palustrine deposits (4–3). These consist of a peculiar pair of black and gray silty levels—dated 340–575 AD—visible on both walls. All are buried under orange-brown colluvial sandy silts (2), with a subhorizontal, thin sandy layer (2a), passing upward to the present pedogenized unit (1).

By comparing and cross-matching the two trench walls, one affected by brittle and the other by ductile deformation, we have reconstructed the depositional and tectonic history of the alluvial-colluvial sequence, as summarize below.

3.2.1. Northern Wall

The 2016 event (E1) is unambiguously revealed by the 20-cm vertical offset of the ground surface, the same value affecting unit 3 top. Moreover, two thin vertical fissures, both filled by silty sands, reach the surface, suggesting the occurrence of liquefaction phenomena. A penultimate event (E2) is suggested by the presence of the dark, organic palustrine layer 4, the deposition of which was likely prompted by the damming of the basin outlet (i.e., by the downthrown of the hanging wall). Unit 4 also seals the displacement of a secondary splay in the hanging wall that, furthermore, affects entirely units 7–5 (F1). The same event is also testified by a larger offset of unit 5 top with respect of the overlaying units (30 versus 20 cm). The last but two events (E3) can be argued by the thickening of the lacustrine layer 7 in the hanging wall, and also by the larger offset (55 versus 30 cm) of the unit 7 bottom with respect to units 5–6. A last but three events (E4) can be only hypothesized by the thickening of unit 9 in the hanging wall.

3.2.2. Southern Wall

The 2016 event (E1) is testified by the set of open fissures affecting the whole succession and by a subdued warping of the uppermost levels (2a). The penultimate event (E2) is revealed by the 0.4-m warping of the lacustrine 7–5 units and of the erosional surface carved above unit 5. Analogously to the northern wall, this warping prompted the damming of the basin, and the formation of a palustrine environment, with the deposition of unit 4 that here also seals a secondary splay affecting the underlying units 7–5 (F1), also supporting the occurrence of E2.

3.3. The Capanna Ghezzi Trench (T3)

This trench (T3 in Figure 4) was opened in a geological context similar to trench T2, with the fault crossing and damming a 0.2-km-long intermontane basin (Figure S15). The 2016 fault rupture affected continuously the western facing slope of the basin, with a N310° strike (Figure 4d), although with smaller vertical offset (0.2–0.35 m) that further decreased in the plain, where it passed to a set of N270° en echelon open fissures with little offset (5–10 cm). We made a 60-m-long ground leveling that quantified the long-wave warping of the alluvial top of the outlet, accounting for a total 1.4-m vertical offset (Figure 9).

The trench was opened with the Hitachi-EX-215 excavator, for a length of 8 m and a depth of 4 m. The unearthed succession was made by both swamp and colluvial deposits, with important pedogenized horizons. The age range has been defined by five AMS dates obtained from detrital charcoals and organic sediment bulks (Table 1).

Above the highly fractured and eroded top of the carbonate basement (unit 7, Maiolica formation), the footwall is mainly made by stiff, ghost-green lacustrine clays (unit 6), suggesting that pedogenic processes occurred below the water table (i.e., hydromorphic pedofacies, characterized by the reduction of iron due to alternating water logging and drainage). In the hanging wall, this peculiar swamp soil is mantled by a wedge-shaped colluvium of sparse carbonate gravels in abundant, reddish oxidized clayey matrix (5), made at expense of the hydromorphic soil in the footwall. The age of this colluvium should be much younger than 16 ka (note the minimum age of sample GHEZ-4 with an unreliable δC13 value; Table 1). The overlying unit 4 is an orange sandy colluvium, with a bulk AMS age of ~8 ka. Upward, it is truncated by a net erosional surface that could match the one affecting unit 6 in the footwall. The entire succession is then mantled by a sandy-silty brown paleosol (unit 3, buried ~2.2 ka), capped by a thin lateritic horizon (2a). Both are buried by a sandy colluvium (2) rich in early Roman pottery fragments, containing a ^{14}C age between 120 BC and 50 AD. The uppermost unit 1 is a sandy-silty palustrine deposit, with sparse carbonate clasts and Middle-Age pottery shards. Upward it is truncated by the excavation for the placing down of an aqueduct pipeline during the twentieth century.

The entire succession is affected by the 2016 open cracks and by a gentle warping due to this ultimate event (E1). A penultimate event (E2) is revealed by the faulting of units 6–2, sealed by the erosional surface es-3 and by the overlying unit 1. The important hiatus between units 4–3 hampers the interpretation of previous events, apart an older one (E6?) that probably occurred a little time before 8.5 ka, as suggested by the presence of colluvial wedge 5.

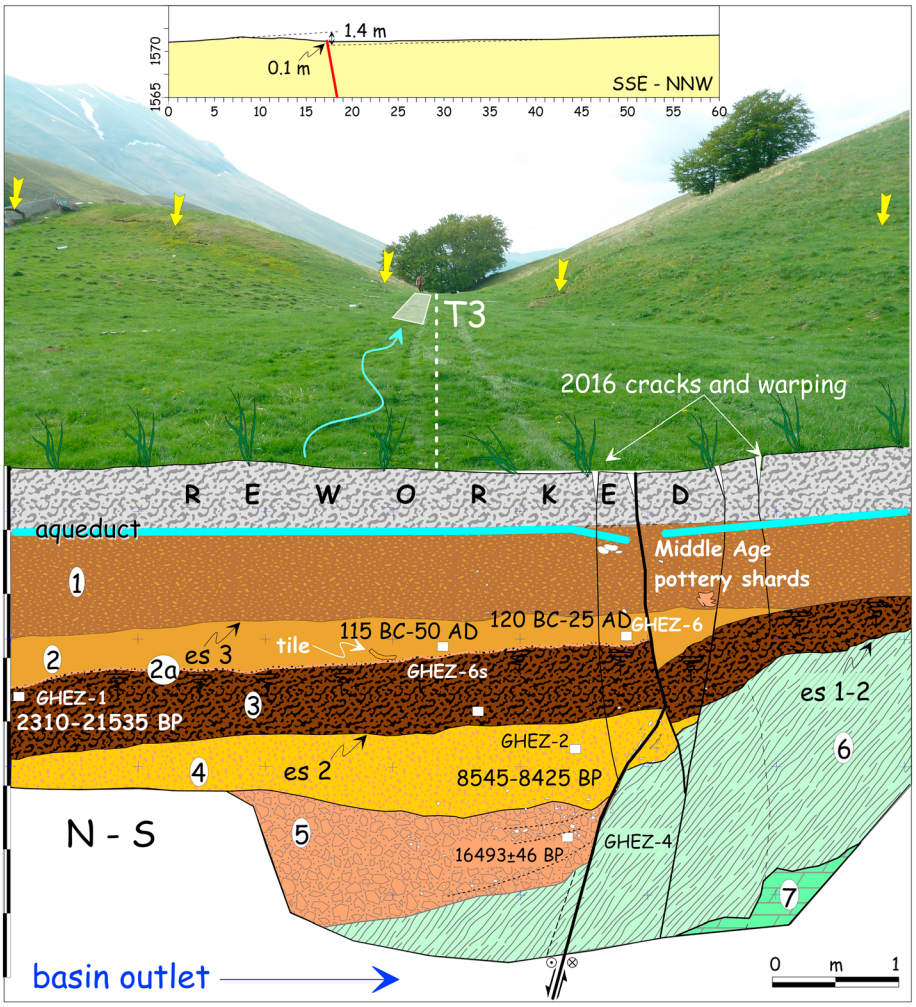

Figure 9. Geological sketch of the eastern wall of trench T3 (see text for unit description). The top panel is a view looking south of the outlet of the small intermontane basin dammed by the fault (yellow arrows indicate the 2016 surface faulting; the faulted house of Figure 4c is at left). White dashed line indicates the ground leveling profile reported above (0.1 m, 2016 coseismic offset; 1.4, cumulated warping). Cyan line indicates the natural basin drainage. Note in the background the Mount Redentore fault scarp.

4. Discussion

Among the eastern silent faults of central Apennine (red in Figure 2a), the MVFS is the only one that possibly released almost all its seismogenic potential after a long quiescence. Knowing the millennial recurrence times of these faults, we did not expect to be eyewitnesses of its awakening in our lives. Today, thanks to the investigations along the poorly known SLF, we are much more aware of the seismogenic behavior of this structure. In fact, by cross-matching the faulting events identified in the three new trenches, and comparing these with the outcomes of the three trenches that Galadini and Galli (2003) opened across the synthetic Prate Pala splay, we can describe more analytically the seismic history of the MVFS. As discussed before, here we assume that these secondary faults, rooted on the main fault at a depth of 1–1.5 km (e.g., in Figure 2d), slip together with the master fault during M_w >6.5 earthquakes. This is confirmed by recent morphometric analyses performed on the Mount Redentore rock fault scarp (Di Donato et al., 2018), which identified three different scarp generations, attributed to the three last surface faulting events described in this paper (i.e., in Galli, Galderisi, et al., 2017).

4.1. Paleoearthquakes

Leaving aside the 2016 event (E1), the penultimate (E2) is now defined better than in Galadini and Galli (2003). Inside T2 (Figure 8), E2 can be constrained as having occurred much after 2.5 kyr BP, but

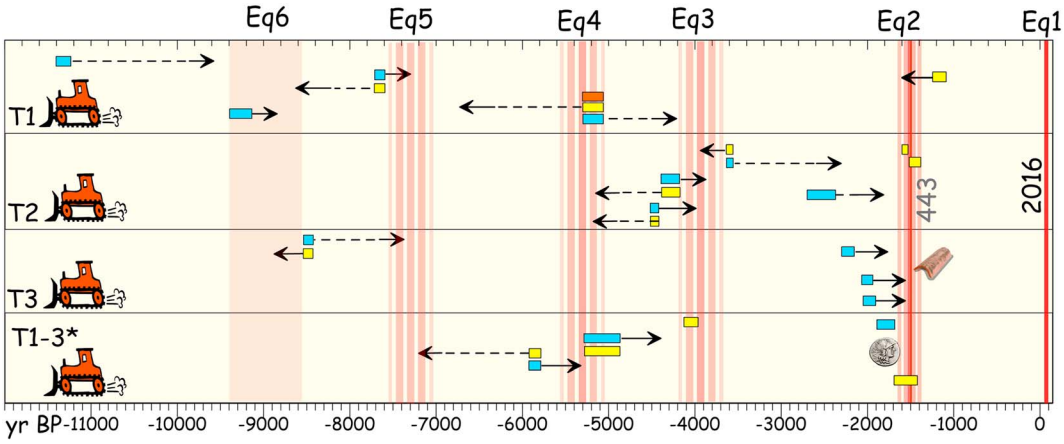

Figure 10. Chronogram of the surface rupture events identified from within the new three trenches (T1–3* are the trenches in Galadini & Galli (2003); BP is 1950 AD)). Colored horizontal bars represent the key samples that bracket the different earthquakes (2σ calibrated interval for ^{14}C ages). Tones suggest *ad quem* (orange), *post quem* (cyan), and *ante quem* (yellow) terms. Horizontal arrows point to the assumed paleoevent age (dashed if related to uncertain indication). Vertical pink bars suggest the most probable earthquake interval (Eq 1–6), as deduced from the samples age, and in the light of the origin of the surrounding deposits (see text for further details). Coin and tale symbols refer to archeological findings that provide age constraints.

immediately before 345–490 AD (1σ, probability sum of the two calibrated ages of SLOR-01 samples), whereas in T3 (Figure 9), it was post 115 BC–50 AD and before the Middle Age, that is, before 690–875 AD in T1. In the old trench 3 it was post 50–265 AD and before 250–540 AD. At the moment, we can place it within the fourth and fifth century (Figure 10).

The last but two events (E3) in T2 occurred between 4.5 and 3.6 kyr BP, whereas in T1 it was a long time after ~5 kyr BP. In the old trench 3, it occurred a long time after 6010–5735 BP and immediately before 4155–3965 BP.

The last but three events (E4) occurred around 5320–5055 BP in T1, and well before ~4.5 kyr BP in T2, whereas in the old trench 1 it was post 5940–5780 BP and ante 5290–4865 BP.

A last but four events in T1 (E5) might have occurred post 7710–7595 BP and ante 5320–5055 BP, whereas it was post 8545–8425 BP in T3.

At the end, an elusive older event (E6) in T1 might have occurred post 9400–9130 BP and before 7710–7595 BP, whereas it was before 8545–8425 BP in T3.

4.1.1. Historical and Archeological Insights on the Penultimate Event

Considering in more detail the E2 age, rough trench data place it in the fourth to fifth century AD, which is in Late Roman period. Although this region of Italy was densely inhabited since the Bronze Age and in Roman times, we have neither historical sources accounting for effects induced by this event, nor archeological evidence from settlements of this period within the near-fault zone. However, at one site, located less than 20 km away from the 2016 epicenter (vs in Figure 1a), archeological excavations found the unambiguous evidence of extensive collapse of the structures belonging to a first-century BC temple (Coarelli & Diosono, 2009). Archeologists dated the ceramic materials involved within the collapse of the temple between the fourth and the fifth century AD, whereas those collected above the rubble leveling start from the second half of the fifth century (F. Diosono, 2017, written communication). The abrupt and simultaneous collapse of this temple can be therefore restricted to the middle of the fifth century. This area, located in the hanging wall of the MVFS, experienced strong shaking also during the 2016 earthquakes, with light-moderate damage to the new, reinforced houses, and several collapses of old, highly vulnerable buildings (Galli, Castenetto, & Peronace, 2017). Therefore, we hypothesize that similar effects occurred to the >400-year-old Roman temple during the penultimate, MVFS earthquake, the age of which can be now narrowed in the midfifth century.

We have a further indication concerning the age of E2. We know that during the Late Antiquity and early Middle-Age—a period with few and poor written sources—there existed some privileged "seismic observatories," monasteries, and few important towns, where earthquakes were annotated. One of these was Rome,

where information concerning seismic events was focused on the effects suffered by the highly vulnerable monuments. In this regard, Galli and Molin (2014) established that all of the monumental buildings in Rome that recorded seismic damage were hit almost exclusively by $M_w > 6.5$ earthquakes sourced by faults located along the Apennine chain, at distances between 90 and 130 km. In facts, in 443 AD, two important and independent historical sources (Fasti Vindobonenses Posteriores, fourth to seventh century; Paulus Diacunus, eighth century) report heavy damage in Rome due to an earthquake, with collapse in many churches and monuments, as in the Colosseum and in Saint Paul basilica (see details in Galli & Molin, 2014). Interestingly, in the same year, another primary source (Annales Ravennates, sixth century) from a different observatory (Ravenna, located 180 km NNW of the MVFS) mentions an earthquake which was felt during the night in the town. Therefore, we can reasonably conclude that these two reports refer to the same earthquake—which was felt in a large part of the Italian peninsula, as happened in 2016 (Galli, Castenetto, & Peronace, 2017)—and that this matches the one sourced around the midfifth century by the MVFS.

4.2. Recurrence Time

In the previous works, MVFS recurrence time was undefined, not longer than 4.7 kyr, and with a minimum elapsed time of 1.4 kyr (Galadini & Galli, 2003). Furthermore, given the conventional years indicated in the Paleoearthquake Catalogue of Italy (Galli et al., 2008), the average recurrence time among the last two events and the present was 2.5 ± 1.4 kyr. Now if we assume that the time spans indicated in the previous section are reliable (Figure 10), return time among different events pairs ranges between 1.4 and 2.3 kyr (for instance, it is 1,573 years between the last two), which gives, on average, ~1.8 ± 0.3 kyr for the last six events. This new estimate of earthquakes recurrence improves substantially the previous one, narrowing the associated uncertainty. This value can be considered typical for Apennine silent faults; for instance, it is similar to the Mount Morrone fault system (southernmost red line in Figure 2a), where Galli et al. (2015) calculated a recurrence time of 2.4 ± 0.2 kyr. In contrast, it is much longer with respect to many structures of the WFS, where paleoseismologically determined return times can be of the order of a few centuries (Galli et al., 2016; Galli & Peronace, 2014). Surprisingly, it is the same of the neighboring Norcia fault (~1.8 ± 0.1 kyr; Galli et al., 2018), the paleoearthquakes of which anticipate by ~0.45 ± 0.15 kyr those sourced by the MVFS. Considering the good completeness of the paleoseismic record of both faults during the Holocene, and also of many other Apennine seismogenic structures, our data do not support the view that these faults are neither slip nor time predictable (e.g., in Benedetti et al., 2013), in agreement with results recently presented by Di Donato et al. (2018) and Galli (2018).

4.3. Late Pleistocene–Holocene Slip Rate

Since we have investigated the antithetic splay of the Mount Vettore master fault, the slip rate of the SLF should be considered a fraction of the MVFS. Also, the slip rates estimated by Galadini and Galli (2003) were minimum values, as they were calculated across the synthetic splay of Prate Pala. Their result from trench analysis was between 0.1 and 0.4 mm/year (0.25 mm/year at least in the past 6 ka), whereas considering the height of the scarp carved over the Prate Pala fan IV, the slip rate was 0.3 ± 0.02 mm/year.

Due to the lack of widespread, Late Quaternary deposits on both sides of the main fault, the evaluation of the MVFS slip rate has always been a problematic task. A very rough attempt can be made by assuming the vertical separation across the straight N140° portion of the rocky fault scarp of the Mount Redentore slope (Figures 2c and 3) as caused by post-LGM, cumulated fault slip (e.g., Dramis, 1983, and discussion in Galli et al., 2012). On the basis of topographic profiles performed on DTM derived from 1:5,000 maps (Figure S16), we calculated that this vertical separation ranges between 8 and 25 m, tapering fast both northward and southward, and being most consistently ~22 m. A secondary fault scarp parallels the main one few hundred meters downhill (see Figure 2c; Civico et al., 2018), showing an average vertical displacement of ~8 m. For both scarps, an amount of this value is represented by the fault slickenside (which must be added by the 2016 rejuvenation), and the remainder by the retreated rock-fault scarp. Considering that (1) part of the scarp might be due to climate exhumation, (2) part of the basal scarp is buried by colluvia, and (3) part of the fault offset cumulated also during the rhexistasy phase which, in the central Apennine, took place before the onset of the LGM (e.g., after 30 ka in Frezzotti & Giraudi (1992)), we can, conservatively, estimate a local slip rate of ~1 mm/year (i.e., ~30 m/~30 kyr). Taking in mind that this sector of the fault experienced the maximum 2016 coseismic offset (up to 2 m on the master fault), and that has the highest Late Pleistocene fault scarps, we consider this slip rate as a local maximum value (Di Donato et al., 2018).

On the other hand, in trenches T2-T3—both located at the tip of the San Lorenzo Fault segments—the 2016 coseismic slip was small (10–20 cm), and therefore, the minimum vertical slip rate in the past 5 ka is only 0.1 mm/year (0.2 mm/year if we consider vertical plus horizontal motion). Conversely, in T1, where the 2016 surface faulting was 0.6–0.8 m, the minimum vertical slip rate in the past 7.5 ka is 0.3 mm/year, whereas—given the 1.4-m vertical separation measured along the ground profile—the vertical slip rate in the past 3.9 ka (i.e., the last two event) is 0.4 mm/year.

By summarizing all the above, one might conclude that the maximum slip rate of the MVFS in the past 30 ka does not exceed 1.3 mm/year in the Mount Redentore segment (rocky fault scarps plus Prate Pala scarp), and is roughly larger than 0.4 mm/year in the rest of the fault system. In other words, the slip rate mimics the 2016 offset distribution along fault, which recorded a peak along the southern segment facing the Piano Grande (e.g., in Figure S16), tapering toward both the system tips (Brozzetti et al., 2019; Civico et al., 2018). According to Manighetti et al. (2005), this triangular, asymmetric shape is characteristic for normal faults, regardless of their scale, and it applies from coseismic slip to long-term fault displacement.

4.4. Maximum Associated Magnitude

The magnitude associated with the entire rupture of the MVFS was calculated by many institutions worldwide in 2016. However, since the rupture occurred during the three main shocks of 24 August (M_w 6.20), 26 October (M_w 6.05), and 30 October (M_w 6.57), by summing the seismic moments of all the strongest events ($M_w > 5.5$ in RCMT (2016)) of the 2016 sequence, applying the Kanamori's (1977) relationship between moment magnitude and seismic moment ($M_w = \log Mo/1.5 - 10.73$), we have

$$M_w = \log\left(1.12\times10^{26}\right)/1.5-10.73 = M_w\ 6.64$$

This is roughly the same value evaluated by applying the Boxer4 code by Galli, Castenetto, and Peronace (2017) on the entire set of macroseismic data points (M_w 6.67 ± 0.07).

On the other hand, in the light of the empirical relationships that link surface rupture length to magnitude, using three regression laws for normal faults, we obtain M_w values slightly higher (0.11–0.17) than summing the three mainshocks.

$$M_w = 4.86 + 1.32 \times \log(30\ \text{km}) = 6.81\ (\text{Wells \& Coppersmith, 1994})$$
$$M_w = 6.12 + 0.47 \times \log(30\ \text{km}) = 6.81\ (\text{Wesnousky, 2008})$$
$$M_w = 4.725 \times (30\ \text{km})\text{^}0.1046 = 6.75\ (\text{Galli et al., 2008})$$

In this regard, one might argue that Galadini and Galli (2003) measured a vertical offset associated with the penultimate event on the Prate Pala splay of 0.45 m versus a maximum of 0.19 m observed in 2016. Leaving aside that slip distribution can vary time by time along the fault, a first possible explanation is that in 2016, the coseismic deformation along the Prata Pale splay was accommodated partly by brittle offset and partly by warping, as revealed by the topographic leveling that evidence 0.5 m of scarp growth (2016 versus 2001 leveling; Figure S1). An alternative and more attractive hypothesis, which makes no claims to being conclusive, is that in the fifth-century earthquake, the different patches composing at depth the MVFS ruptured all together, and not in three different times as in 2016 (Chiaraluce et al., 2017; Scognamiglio et al., 2018), generating one higher-magnitude earthquake ($M_w \geq 6.64$), higher surface slips, and higher shaking both in the near and far field (e.g., in Rome and Ravenna).

5. Conclusion

The M_w 6.6 earthquake in central Italy was sourced by the 30-km-long MVFS, one of the four major historically silent normal faults of the Apennines. The fault ruptured at surface for dozens of kilometers, with offset exceeding 2 m in places. Since the master fault runs mainly along the steep carbonate slopes of the Sibillini range or alongside its highest, sharp ridge, where the lack of fine, datable sediments and the abundance of rock debris would surely undo paleoseismological analyses, here we focused our investigations along the SLF. This is the main antithetic segment that ruptured at surface for 5 km on 30 October, allowing us to open three paleoseismological trenches inside swamp and colluvial deposits affected by faulting. Thanks to 19

AMS ages of charcoals and organic sediments sampled within trenches, by comparing the faulting evidence collected here with those published by Galadini and Galli (2003) along a synthetic splay of the master fault (Prate Pala Fault), we have delineated—for the first time—the Holocene seismic history of the MVFS.

Overall, we recognized six surface faulting events (including the 2016 one) which occurred in the past 9 kyr, with an average return period of 1.8 ± 0.3 kyr, for $M_w \geq 6.6$ earthquakes. The penultimate event was dated in the midfifth century AD, and we associate it with the 443 AD earthquake recorded by historical accounts for being strongly felt in Ravenna, and for damaging important monuments in Rome. Giving these time spans, in hindsight one could say that the 2016 earthquake was not so unexpected as previously supposed. In facts, the elapsed time since the penultimate event (1,573 years) falls within the lower boundary of the recurrence period of such class of events.

We have also defined the slip rate of the MVFS, with data mainly deriving from the splays facing Piano Grande di Castelluccio. By summing the values of the master fault with those of the secondary faults we obtained a maximum rate of 1.3 mm/year focused in the area that experienced also the maximum coseismic slip (surficial and at depth) and the maximum seismic moment release.

If in the aftermath of the 2016 earthquake it was possible to say that the MVFS was one of the very few faults in the world that ruptured at surface after that early paleoseismological trenching revealed its existence and quantified its activity, now we can conclude that this kind of analyses, when joined with Quaternary studies, is still the best way to unambiguously investigate and characterize the seismogenic behavior of an active fault. Since the largest earthquakes that threaten Italy, and many other region of the globe, recur hundreds or thousands of year apart, only paleoseismology can provide long-term rates of occurrence needed by the national map that forecast seismic shaking at various probability levels. Although it might sound obvious, this study shows clearly that our seismic hazard perception, the ability of forecasting, and hence planning risk mitigation can be strongly supported by our geological knowledge of the behavior of active faults.

Acknowledgments
We are grateful to F. Diosono and F. Coarelli for the discussion on the archeological evidence of Villa San Silvestro. In particular, F. Diosono shared with us her latest data concerning the destruction/reconstruction phases of the Roman settlement. We thank C. Bifulco and A. Rossetti of the National Park of Monti Sibillini for the quick trenching permission. We are grateful to R. Marinelli and E. Lucci of S.E.A. (Cascia) who sponsored and made the excavation of trenches 1 and 2. Thanks to S. Nomade (CEA Saclay) for providing us some ^{14}C ages. The data used are listed in figures, supporting information, and references. The database of ground surface rupture is available at https://doi.org/10.1594/PANGAEA.879469. The important criticisms by two anonymous reviewers enhanced the final version of the manuscript. The views and conclusions contained here are those of the authors and should not be interpreted as necessarily representing official policies, either expressed or implied, of the Italian government.

References

Battaglia, M., Murray, M. H., Serpelloni, E., & Bürgmann, R. (2004). The Adriatic region: An independent microplate within the Africa-Eurasia collision zone. *Geophysical Research Letters*, *31*, L09605. https://doi.org/10.1029/2004GL019723

Benedetti, L., Manighetti, I., Gaudemer, Y., Finkel, R., Malavieille, J., Pou, K., et al. (2013). Earthquake synchrony and clustering on Fucino faults (Central Italy) as revealed from in situ 36Cl exposure dating. *Journal of Geophysical Research: Solid Earth*, *118*, 4948–4974. https://doi.org/10.1002/jgrb.50299

Boncio, P., Lavecchia, G., & Pace, B. (2004). Defining a model of 3D seismogenic sources for seismic hazard assessment applications: The case of central Apennines (Italy). *Journal of Seismology*, *8*(3), 407–425. https://doi.org/10.1023/B:JOSE.0000038449.78801.05

Bosi, C., Galadini, F., Giaccio, B., Messina, P., & Sposato, A. (2003). Plio-Quaternary continental deposits in the Latium-Abruzzi Apennines: The correlation of geological events across different intermontane basins. *Italian Journal of Quaternary Sciences*, *16*, 55–76.

Brozzetti, F., Boncio, P., Cirillo, D., Ferrarini, F., de Nardis, R., Testa, A., et al. (2019). High-resolution field mapping and analysis of the August–October 2016 coseismic surface faulting (central Italy earthquakes): Slip distribution, parameterization, and comparison with global earthquakes. *Tectonics*, *38*. https://doi.org/10.1029/2018TC005305

Calamita, F., & Pizzi, A. (1994). Recent and active extensional tectonics in the southern Umbro-Marchean Apennines (central Italy). *Memorie della Societa Geologica Italiana*, *48*, 541–548.

Calamita, F., Pizzi, A., & Roscioni, M. (1992). I fasci di faglie recenti ed attive di M. Vettore-M. Bove e di M. Castello-M. Cardosa (Appennino Umbro-Marchigiano), *St. Geol. Cam., special issue* 1992*/1*, 81–95.

Carminati, E., Lustrino, M., & Doglioni, C. (2012). Geodynamic evolution of the central and western Mediterranean: Tectonics vs. igneous petrology constraints. *Tectonophysics*, *579*, 173–192. https://doi.org/10.1016/j.tecto.2012.01.026

Cello, G., Mazzoli, S., Tondi, E., & Turco, E. (1997). Active tectonics in the central Apennines and possible implications for seismic hazard analysis in peninsular Italy. *Tectonophysics*, *272*(1), 43–68. https://doi.org/10.1016/S0040-1951(96)00275-2

Cheloni, D., de Novellis, V., Albano, M., Antonioli, A., Anzidei, M., Atzori, S., et al. (2017). Geodetic model of the 2016 central Italy earthquake sequence inferred from InSAR and GPS data. *Geophysical Research Letters*, *44*, 6778–6787. https://doi.org/10.1002/2017GL073580

Chiaraluce, L., Di Stefano, R., Tinti, E., Scognamiglio, L., Michele, M., Casarotti, E., et al. (2017). The 2016 central Italy seismic sequence: A first look at the mainshocks, aftershocks, and source models. *Seismological Research Letters*, *88*(3), 757–771. https://doi.org/10.1785/0220160221

Civico, R., Pucci, S., Villani, F., Pizzimenti, L., De Martini, P. M., Nappi, R., & the Open EMERGEO Working Group (2018). Surface ruptures following the 30 October 2016 M_w 6.5 Norcia earthquake, central Italy. *Journal of Maps*, *14*(2), 151–160. https://doi.org/10.1080/17445647.2018.1441756

Clark, P. U., Dyke, A. S., Shakun, J. D., Carlson, A. E., Clark, J., Wohlfarth, B., et al. (2009). The last glacial maximum. *Science*, *325*(5941), 710–714. https://doi.org/10.1126/science.1172873

Coarelli, F., & Diosono, F. (2009). *I Templi e il Forum di Villa S. Silvestro. La Sabina dalla conquista romana a Vespasiano*. Roma: Edizioni Quasar.

Cowie, P., Phillips, R., Roberts, G., McCaffrey, K., Zijerveld, L., Gregory, L., et al. (2017). Orogen-scale uplift in the central Italian Apennines drives episodic behaviour of earthquake faults. *Scientific Reports*, *7*, 44858. https://doi.org/10.1038/srep44858

D'Agostino, N. (2014). Complete seismic release of tectonic strain and earthquake recurrence in the Apennines (Italy). *Geophysical Research Letters*, *41*, 1155–1162. https://doi.org/10.1002/2014GL059230

D'Agostino, N., Avallone, A., Cheloni, D., D'Anastasio, E., Mantenuto, S., & Selvaggi, G. (2008). Active tectonics of the Adriatic region from GPS and earthquake slip vectors. *Journal of Geophysical Research*, *113*, B12413. https://doi.org/10.1029/2008JB005860

D'Agostino, N., Jackson, J. A., Dramis, F., & Funiciello, R. (2001). Interactions between mantle upwelling, drainage evolution and active normal faulting: an example from the central Apennines (Italy). *Geophysical Journal International*, *147*(2), 475–497.

Di Donato, M., Boncio, P., Mataloni, G., Testa, A., Palumbo, D., Le Donne, L. (2018). Evidenze di paleodislocazioni cosismiche lungo la faglia di M. Vettore (Italia centrale) rivelate da analisi topografiche di dettaglio della scarpata di faglia su roccia, Extended abstracts of the 37° GNGTS Congress, Bologna 19–21 November 2018 (pp. 46–48).

Doglioni, C., Mongelli, F., & Pieri, P. (1994). The Puglia uplift (SE Italy): An anomaly in the foreland of the Apenninic subduction due to buckling of a thick continental lithosphere. *Tectonics*, *13*(5), 1309–1321. https://doi.org/10.1029/94TC01501

Dramis, F. (1983). Morfogenesi di versante nel Pleistocene superiore in Italia: I depositi detritici stratificati. *Geografia Fisica e Dinamica Quaternaria*, *6*, 180–182.

Ferrario, M. F., & Livio, F. (2018). Characterizing the distributed faulting during the 30 October 2016, central Italy earthquake: A reference for fault displacement hazard assessment. *Tectonics*, *37*, 1256–1273. https://doi.org/10.1029/2017TC004935

Frezzotti, M., & Giraudi, C. (1992). Evoluzione geologica tardo-pleistocenica ed olocenica del conoide complesso di Valle Majelama (Massiccio del Velino-Abruzzo). *Quaternario*, *5*, 33–50.

Galadini, F., & Galli, P. (2000). Active tectonics in the central Apennines (Italy)—Input data for seismic hazard assessment. *Natural Hazards*, *22*(3), 225–268. https://doi.org/10.1023/A:1008149531980

Galadini, F., & Galli, P. (2003). Paleoseismology of silent faults in the central Apennines (Italy): The Mt. Vettore and Laga Mts. Faults. *Annals of Geophysics*, *46*, 815–836.

Galli, P. (2018). Conosci le tue faglie e il prossimo tuo, extended abstracts of the 37° GNGTS Congress, Bologna, November 2018 (pp. 122–125).

Galli, P., Castenetto, S., & Peronace, E. (2017). The macroseismic intensity distribution of the 30 October 2016 earthquake in Central Italy (M_w 6.6): Seismotectonic implications. *Tectonics*, *36*, 2179–2191. https://doi.org/10.1002/2017TC004583

Galli, P., & Galadini, F. (1999). Seismotectonic framework of the 1997–98 Umbria-Marche (central Italy) earthquakes. *Seismological Research Letters*, *70*, 404–414.

Galli, P., Galadini, F., & Pantosti, D. (2008). Twenty years of paleoseismology in Italy. *Earth-Science Reviews*, *88*(1-2), 89–117. https://doi.org/10.1016/j.earscirev.2008.01.001

Galli, P., Galderisi, A., Ilardo, I., Piscitelli, S., Scionti, V., Bellanova, J., & Calzoni, F. (2018). Holocene paleoseismology of the Norcia fault system (central Italy). *Tectonophysics*, *745*, 154–169. https://doi.org/10.1016/j.tecto.2018.08.008

Galli, P., Galderisi, A., Peronace, E., Giaccio, B., Hajdas, I., Messina, P., & Polpetta, F. (2017). Quante volte figliola? Confessioni sibilline di una giovane faglia, *Extended abstracts of the 36° GNGTS Congress,* Trieste, November 2017 (pp. 41–45).

Galli, P., Giaccio, B., Messina, M., & Peronace, E. (2016). Three magnitude 7 earthquakes on a single fault in central Italy in 1400 years, evidenced by new palaeoseismic results. *Terra Nova*, *28*(2), 146–154. https://doi.org/10.1111/ter.12202

Galli, P., Giaccio, B., & Messina, P. (2010). The 2009 central Italy earthquake seen through 0.5 Myr-long tectonic history of the L'Aquila faults system. *Quaternary Science Reviews*, *29*(27-28), 3768–3789. https://doi.org/10.1016/j.quascirev.2010.08.018

Galli, P., Giaccio, B., Messina, P., Peronace, E., & Zuppi, G. M. (2011). Paleoseismology of the L'Aquila faults (central Italy, 2009 M_w 6.3 earthquake): Implications for active fault linkage. *Geophysical Journal International*, *187*(3), 1119–1134. https://doi.org/10.1111/j.1365-246X.2011.05233.x

Galli, P., Giaccio, B., Peronace, E., & Messina, P. (2015). Holocene Paleoearthquakes and Early-Late Pleistocene slip rate on the Sulmona fault (central Apeninnes, Italy). *Bulletin of the Seismological Society of America*, *105*(1), 1–13. https://doi.org/10.1785/0120140029

Galli, P., Messina, P., Giaccio, B., Peronace, E., & Quadrio, B. (2012). Early Pleistocene to late Holocene activity of the Magnola fault (Fucino fault system, central Italy). *Bollettino di Geofisica Teorica ed Applicata*, *53*, 435–458.

Galli, P., & Molin, D. (2014). Beyond the damage threshold: The historic earthquakes of Rome. *Bulletin of Earthquake Engineering*, *12*(3), 1277–1306. https://doi.org/10.1007/s10518-012-9409-0

Galli, P., & Peronace, E. (2014). New paleoseismic data from the Irpinia fault. A different seismogenic perspective for southern Apennines (Italy). *Earth-Science Reviews*, *136*, 175–201. https://doi.org/10.1016/j.earscirev.2014.05.013

Galli, P., Peronace, E., Quadrio, B., & Esposito, G. (2014). Earthquake fingerprints along fault scarps: A case study of the Irpinia 1980 earthquake fault (southern Apennines). *Geomorphology*, *206*, 97–106. https://doi.org/10.1016/j.geomorph.2013.09.023

Giaccio, B., Galli, P., Messina, P., Peronace, E., Scardia, G., Sottili, G., et al. (2012). Fault and basin depocentre migration over the last 2 Ma in the L'Aquila 2009 earthquake region, central Italian Apennines. *Quaternary Science Reviews*, *56*, 69–88. https://doi.org/10.1016/j.quascirev.2012.08.016

Giraudi, C. (2003). I depositi alluvionali olocenici di Campo Imperatore (massiccio del Gran Sasso – Abruzzo). *Italian Journal of Quaternary Sciences*, *16*, 197–205.

Giraudi, C. (2005). Late-Holocene alluvial events in the central Apennines, Italy. *The Holocene*, *15*(5), 768–773. https://doi.org/10.1191/0959683605hl850rr

Kanamori, H. (1977). The energy release in great earthquakes. *Journal of Geophysical Research*, *82*(20), 2981–2987. https://doi.org/10.1029/JB082i020p02981

Lavecchia, G., Brozzetti, F., Barchi, M., Menichetti, M., & Keller, J. V. A. (1994). Seismotectonic zoning in east-central Italy deduced from an analysis of the Neogene to present deformations and related stress fields. *Geological Society of America Bulletin*, *106*(9), 1107–1120. https://doi.org/10.1130/0016-7606(1994)106<1107:SZIECI>2.3.CO;2

Manighetti, I., Campillo, M., Sammis, C., Mai, P. M., & King, G. (2005). Evidence for self-similar, triangular slip distributions on earthquakes: Implications for earthquake and fault mechanics. *Journal of Geophysical Research*, *110*, B05302. https://doi.org/10.1029/2004JB003174

Molin, D., Galadini, F., Galli, P., Mucci, L., & Rossi, A. (1999). Terremoto del Fucino del 13 gennaio 1915. Studio macrosismico. In S. Castenetto, & F. Galadini (Eds.), *13 gennaio 1915. Il terremoto nella Marsica* (pp. 321–340, 631–661). Roma: Istituto Poligrafico e Zecca dello Stato

Patacca, E., Sartori, R., & Scandone, P. (1990). Tyrrhenian basin and Apenninic arcs: Kinematic relations since late Tortonian times. *Memorie della Societa Geologica Italiana*, *45*, 425–451.

Patacca, E., Scandone, P., Di Luzio, E., Cavinato, G. P., & Parotto, M. (2008). Structural architecture of the central Apennines: Interpretation of the CROP 11 seismic profile from the Adriatic coast to the orographic divide. *Tectonics*, *27*, TC3006. https://doi.org/10.1029/2005TC001917

Pierantoni, P. P., Deiana, G., & Galdenzi, S. (2013). *Geological Map of the Sibillini Mountains (Umbria-Marche Apennines, Italy)*. Firenze: Litografia Artistica Cartografica.

Pizzi, A., Calamita, F., Coltorti, M., & Pieruccini, P. (2002). Quaternary normal faults, intramontane basins and seismicity in the Umbria-Marche-Abruzzi Apennine ridge (Italy): Contribution of neotectonic analysis to seismic hazard assessment. *Bollettino Della Società Geologica Italiana*, *1*, 923–929.

Pizzi, A., Di Domenica, A., Gallovič, F., Luzi, L., & Puglia, R. (2017). Fault segmentation as constraint to the occurrence of the main shocks of the 2016 central Italy seismic sequence. *Tectonics*, *36*, 2370–2387. https://doi.org/10.1002/2017TC004652

RCMT (2016). European-Mediterranean RCMT catalog. Retrived from http://autorcmt.bo.ingv.it/QRCMT-on-line/QRCMT16-on-line/lista2016.html

Roberts, G. P., & Michetti, A. M. (2004). Spatial and temporal variations in growth rates along active normal fault systems: An example from the Lazio-Abruzzo Apennines, central Italy. *Journal of Structural Geology*, *26*(2), 339–376. https://doi.org/10.1016/S0191-8141(03)00103-2

Scognamiglio, L., Tinti, E., Casarotti, E., Pucci, S., Villani, F., Cocco, M., et al. (2018). Complex fault geometry and rupture dynamics of the M_w 6.5, 2016, October 30th central Italy earthquake. *Journal of Geophysical Research: Solid Earth*, *123*, 2943–2964. https://doi.org/10.1002/2018JB015603

TDMT (2018). Catalogue of time domain moment tensor. Retrieved from http://cnt.rm.ingv.it/tdmt

Villani, F., Pucci, S., Civico, R., De Martini, P. M., Cinti, F. R., & Pantosti, D. (2018). Surface faulting of the 30 October 2016 M_w 6.5 central Italy earthquake: Detailed analysis of a complex coseismic rupture. *Tectonics*, *37*, 3378–3410. https://doi.org/10.1029/2018TC005175

Villani, F., & Sapia, V. (2017). The shallow structure of a surface-rupturing fault in unconsolidated deposits from multi-scale electrical resistivity data: The 30 October 2016 M_w 6.5 central Italy earthquake case study. *Tectonophysics*, *717*, 628–644. https://doi.org/10.1016/j.tecto.2017.08.001

Wallace, R. E. (1980). Degradation of the Hebgen Lake fault scarps of 1959. *Geology*, *8*(5), 225–229. https://doi.org/10.1130/0091-7613(1980)8<225:DOTHLF>2.0.CO;2

Wells, D. L., & Coppersmith, K. J. (1994). New empirical relationships among magnitude, rupture length, rupture width, rupture area, and surface displacement. *Bulletin of the. Seismological Society of America*, *84*, 974–1002.

Wesnousky, S. (2008). Displacement and geometrical characteristics of earthquake surface ruptures: Issues and implications for seismic-Hazard analysis and the process of earthquake rupture. *Bulletin of the Seismological Society of America*, *98*(4), 1609–1632. https://doi.org/10.1785/0120070111

Wilkinson, M. W., McCaffrey, K. J. W., Jones, R., Roberts, G., Holdsworth, R., Gregory, L., et al. (2017). Near-field fault slip of the 2016 Vettore M_w 6.6 earthquake (central Italy) measured using low-cost GNSS. *Scientific Reports*, *7*(4612), 7.

Yeats, R. S., Sieh, K., & Allen, C. R. (1997). *The Geology of Earthquakes* (p. 568). New York and Oxford: Oxford University Press.

Zanchetta, G., Giraudi, C., Sulpizio, R., Magny, M., Drysdale, R., & Sadori, L. (2012). Constraining the onset of the Holocene "Neoglacial" over the central Italy using tephra layers. *Quaternary Research*, *78*(02), 236–247. https://doi.org/10.1016/j.yqres.2012.05.010